Capacity of OFDM Systems over Fading Underwater Acoustic Channels

Authors: Chantri Polprasert, *Member, IEEE*, James A. Ritcey, *Fellow, IEEE*, and Milica Stojanovic, *Fellow, IEEE*
Publication: IEEE Journal of Oceanic Engineering, vol. 36, no. 4, Oct. 2011
Speaker: Zafar Iqbal

Short Summary:

This paper derives the upper and lower bounds for channel capacity of the OFDM systems over underwater acoustic channels as a function of distance between the transmitter and the receiver. The upper bound is obtained using perfect CSI at the receiver while the lower bound is obtained by assuming that the input is drawn from a PSK constellation which results in non-Gaussian distribution of the output signal and no CSI. It incorporates frequency dependent path loss at each arrival path at the receiver due to acoustic propagation. This leads the UW channel to be modeled as wide sense stationary and correlated scattering (WSS-non-US) fading channel. Results from both Rayleigh and Rician fading show a gap between the upper and lower bounds which depends, not only on the ranges and shape of the scattering function of the UW channel but also on the distance between the transmitter and the receiver.

I. INTRODUCTION

Recently, OFDM has been applied to the UWA communications and yields high data rate with strong bit error rate performance [2-5].

Time and frequency spreading are the main challenges for data transmission through UW channels. Several attempts have been made to characterize the UW channel, most of which view the UW channel as a linear time-varying channel with wide sense stationary and uncorrelated scattering (WSSUS) [8-10]. However, this approach treats the entire frequency band as a whole and neglects the frequency dependent path loss. This model is acceptable for transmissions at low bandwidth (<10 kHz) [9].

Channel capacity over WSSUS fading channel has been studied [12-15] under these assumptions: 1) no CSI is available at the transmitter or receiver, and 2) peak power constraints. It is shown that channel capacity is achieved at capacity maximizing bandwidth, which depends

on the ranges and shape of the scattering function of the fading channel. These studies are conducted over wireless fading channels which assume constant power spectral density (PSD) and AWGN noise. There has been some research on the capacity of UW channels [6, 16, 17] but all assume no fading in their UW channels.

This paper investigates the capacity of OFDM systems over the UW fading channels with no CSI at the transmitter or the receiver. The UW channel is modeled by taking into account frequency-dependent path loss. This invalidates the assumption of stationarity in frequency of the WSSUS model and leads to a frequency-dependent doubly spread (DS) fading channel characterized by the WSS-non-US [18] assumptions. The conventional WSSUS model is uncorrelated in both delay and Doppler domains but the proposed model is uncorrelated in the Doppler domain and correlated in the delay domain.

Using this channel model and assuming that the acoustic propagation and ambient noise PSD are available at both the transmitter and receiver, capacity upper and lower bounds are derived. Capacity upper bound is derived by assuming perfect CSI at the receiver, while lower bound is obtained by the mutual information rate whose input is an i.i.d. random variable and is drawn from a PSK modulation [12,19], which results in a non-Gaussian distribution of the output signal. Results are obtained for both Rayleigh and Rician fading of the UW channel. Simulation results show a gap between the upper and lower bounds which depends not only on the ranges and shape of the scattering function of the UW channel, but also on the distance between the transmitter and receiver. Results are confirmed with the scattering function obtained from the 2008 rescheduled Acoustic Communications Experiment (RACE08) experimental data.

II. OFDM System and UW Channel Model

In this section, an OFDM system model for UW acoustic communications is developed. Physical and statistical properties of the channel as well as PSD of the ambient noise are investigated and a frequency-dependent UW DS fading channel has been proposed.

A. OFDM System

A conventional CP-OFDM system is considered as shown in Fig. 1. Let $\mathbf{X}_n = \left[X_{n,0} ... X_{n,K-1} \right]^T$ and $\mathbf{Y}_n = \left[Y_{n,0} ... Y_{n,K-1} \right]^T$ be the sent and received block of data at the *n*th OFDM symbol duration, respectively.

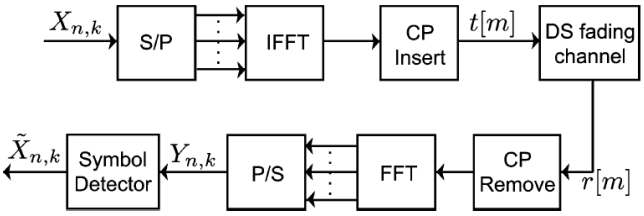

Fig. 1. System model

Assuming the guard interval L_{cp} is longer than the channel length L to avoid the interblock interference (IBI), the input/output relationship can be written as,

$$Y_{n,k} = G_{n,k}(d) X_{n,k} + N_{n,k} \tag{1}$$

where $k \in [0,...,K-1]$ is the subcarrier index and $n \in [0,...,N-1]$, while d is the distance between transmitter and receiver. $G_{n,k}(d)$ denotes the channel transfer function at the kth subcarrier. $N_{n,k}$ is the ambient noise in the ocean. This simplifies the fading effect into multiplicative coefficient, which is the basis for analysis of the UW channel in this paper. The impact of ICI is assumed to be negligible through appropriate parameter settings (Justified in App. I). For simplicity, the overall system input/output of the entire N OFDM transmissions is characterized by a vector of size $NK \times 1$, as follows.

$$\mathbf{Y} = \text{diag}(\mathbf{X})\mathbf{G}(d) + \mathbf{N} = \text{diag}(\mathbf{G}(d))\mathbf{X} + \mathbf{N} \tag{2}$$

where

$$\mathbf{Y} = \left[\mathbf{Y}_0^T ... \mathbf{Y}_{N-1}^T \right]^T \text{ and } \mathbf{Y}_n = \left[Y_{n,0} ... Y_{n,K-1} \right]^T \tag{3}$$

$$\mathbf{X} = \left[\mathbf{X}_0^T ... \mathbf{X}_{N-1}^T \right]^T \text{ and } \mathbf{X}_n = \left[X_{n,0} ... X_{n,K-1} \right]^T \tag{4}$$

$$\mathbf{N} = \left[\mathbf{N}_0^T ... \mathbf{N}_{N-1}^T \right]^T \text{ and } \mathbf{N}_n = \left[N_{n,0} ... N_{n,K-1} \right]^T \tag{5}$$

$$\mathbf{G}(d) = \left[\mathbf{G}_0^T(d) ... \mathbf{G}_{N-1}^T(d) \right]^T \text{ and } \mathbf{G}_n(d) = \left[G_{n,0}(d) ... G_{n,K-1}(d) \right]^T \tag{6}$$

B. Characterization of Approximate DS Fading Channels

UW channel is modeled using both the physical property, which is the attenuation depending on the propagation distance and bandwidth of the transmitted signal, and the statistical property for which the channel is usually assumed WSSUS.

1) Frequency-dependent Path Loss

For the signal propagated through UW medium, the attenuation or path loss, which is a function of distance and signal frequency, is a combination of geometric spreading and absorption, written as,

$$Q^2(d, f) = d^{-sp}(q^2(f))^{-d} \tag{7}$$

where d is the propagated distance in meter and f is the frequency in kilohertz. d^{-sp} represents the spreading loss and sp is the spreading factor which is set to 1.5. $q^2(f)$ is the absorption coefficient in seawater which is given by,

$$10\log(q^2(f)) = 2.49\times10^{-7} f^2 + 0.99\frac{f^2}{f^2+1.23\times10^4} + 1.48\times10^{-4}\frac{f^2}{f^2+1.522} \text{ dB/m} \tag{8}$$

Eq. (8) is calculated when the salinity S is 35 parts per thousand (ppt), gauge pressure P_a is 1 atm, temperature T=14 ^{o}C, and the relaxation frequency is 111 kHz.

2) Conventional Statistical Model

The CIR is modeled by a sum of several multipath components [9], [10]. Let $h(t, \tau)$ denote a continuous-time CIR of linear time-variant (LTV) UW channels and its corresponding transfer function $H(t, f)$ is,

$$h(t,\tau) = \sum_{i=0}^{I-1} h_i(t)\delta(\tau-\tau_i), \quad H(t, f) = \sum_{i=0}^{I-1} h_i(t)e^{-j2\pi f\tau_i} \tag{9}$$

where I is the number of arrival paths. WSSUS is commonly assumed to characterize the channel, i.e., $E\{h[t,\tau]h^*[t',\tau']\} = R_{h_c}(t-t',\tau)\delta(\tau-\tau')$ where $R_{h_c}(t-t',\tau)$ is the autocorrelation function of the delay τ between time t and t'. Its corresponding scattering function is $S_c(\tau, v) = \int R_{h_c}(\Delta t,\tau)\exp(-j2\pi\Delta tv)d\Delta t$ where $\tau \in [0, \tau_m]$. For a bandwidth of less than 10 kHz, let τ_m and f_d denote the maximum channel delay spread and 3-dB Doppler spread of $S_c(\tau,v)$, respectively.

3) Frequency-dependent DS Fading Channels

Conventionally, UW models use WSSUS properties to characterize LTV UW channels, assuming equal attenuation across all the signal bandwidth, treating the entire frequency band as

flat and neglecting frequency-dependent parameters of the individual arrival path. In reality, various factors from channel physics such as the attenuation, reflection loss, or tx/rx operating ranges influence frequency dependency on the path loss. In this paper, the impact of channel physics is limited to only the attenuation $Q^2(d_i, f)$ (7) where d_i is the propagation distance of ith delay path.

Let $\chi_{d_i}(\tau)$ denote a CIR of the ith delay path corresponding to $Q(d_i, f)$ i.e., $Q(d_i, f) = \int \chi_{d_i}(\tau)\exp(-j2\pi f\tau)d\tau$ where $Q^2(d_i, f) = Q(d_i, f)Q^*(d_i, f)$. Taking into account $\chi_{d_i}(\tau)$ yields a modified CIR, $g_d(t, \tau)$

$$g_d(t,\tau) = \sum_{i=0}^{I-1} h_i(t)\chi_{d_i}(\tau) \otimes \delta(\tau - \tau_i) \tag{10}$$

$$\begin{aligned} G_d(t, f) &= \int g_d(t,\tau)e^{-j2\pi\tau f}d\tau \\ &= \sum_{i=0}^{I-1} h_i(t)Q(d_i, f)e^{-j2\pi\tau_i f} \\ &\approx Q(d0, f)\sum_{i=0}^{I-1} h_i(t)e^{-j2\pi\tau_i f} \quad \because Q(d, f) \approx Q(d_{I-1}, f) \\ &= Q(d, f)H(t, f) \end{aligned} \tag{11}$$

d_0 is the distance between transmitter and receiver and the subscript of d is neglected for simplicity. Hence the modified CIR is

$$g_d(t,\tau) = \chi_d(\tau) \otimes \sum_{i=0}^{I-1} h_i(t)\delta(\tau - \tau_i) \tag{12}$$

From the sampling theorem, the T_s-spaced discrete time CIR is,

$$\begin{aligned} g_{0,d}[m, p_l] &= \int_{\tau} g_d(mT_s, \tau)\,\mathrm{sinc}(B\tau - p_l)d\tau \\ &\approx g_d(mT_s, p_lT_s) \quad \because B \text{ is large} \\ &= \chi_d[l] \otimes h_0[m, p_l] \end{aligned} \tag{13}$$

where B=1/T_s. From (13) the channel transfer function can be written as

$$
\begin{aligned}
G_{n,k}(d) &= \sum_{m'=0}^{K-1}\left(\frac{1}{K}\sum_{l=0}^{L-1} g_{0,d}^{n}\left[m'+L_{cp},l\right]\sum_{p=0}^{K-1} e^{j2\pi p(m'-l)/K}\right)\times e^{-j2\pi m'k/K} \\
&= \sum_{p=0}^{K-1}\sum_{l=0}^{L-1}\left(\frac{1}{K}\sum_{m'=0}^{K-1}\left(\chi_d[l]\otimes h_0^n\left[m'+L_{cp},l\right]\right)\times e^{j2\pi m'(p-k)/K}\right)e^{-j2\pi pl/K} \\
&\approx \sum_{p=0}^{K-1}\sum_{l=0}^{L-1} G_{n,l}^{d}[0]e^{-j2\pi kl/K} \\
&= Q(d,f_k)H_{n,k}
\end{aligned}
\tag{14}
$$

where $f_k = f_c + k/(KT_s)$ and f_c is the center frequency corresponding to the zeroth subcarrier. $g_{0,d}^{n}\left[m',l\right] = g_{0,d}\left[nN_s + p_0 + m', p_l\right]$ and $h^n[m',l] = h_0\left[nN_s + p_0 + m', p_l\right]$ where $N_s = L_{cp} + K$ is the OFDM symbol length and p_0 is the arrival time of the first arrival path. Eq. (14) is derived under negligible ICI. Moreover,

$$
\begin{aligned}
H_{n,k} &= \sum_{l=0}^{L-1}\left(\frac{1}{K}\sum_{m'=0}^{K-1} h_0^n\left[m'+L_{cp},l\right]\right)e^{-j2\pi lk/K} \\
&= \sum_{l=0}^{L-1} h_{n,l}[0]e^{-j2\pi lk/K}
\end{aligned}
\tag{15}
$$

$$
Q(d,f_k) = \sum_{l=0}^{L-1}\chi_d[l]e^{-j2\pi lk/K} \tag{16}
$$

and

$$
G_{n,l}^{d}[p-k] = \frac{1}{K}\sum_{m'=0}^{K-1}\left(\chi_d[l]\otimes h_0^n\left[m'+L_{cp},l\right]\right)e^{j2\pi m'(p-k)/K} \tag{17}
$$

$G_{n,k}(d)$ is the fading gain encountered by the signal transmitted on the kth subcarrier. $Q(d, f_k)$ is assumed constant within a subcarrier with center frequency f_k. $H_{n,k}[0]$ is the approximate CIR. Eq. (14) simplifies the transfer function of frequency-dependent UW DS channel into a multiplication of the attenuation $Q(d,f_k)$ and statistical part $H_{n,k}$ governed by the scattering function $S[l, \lambda]$. Assuming $S[l,\lambda] \approx S_c\left(lT_s, \lambda/T_b\right)$ when the variation of $h_0[m, p_l]$ within $T_b(T_b=N_sT_s)$ is negligible [32]. T_b is the OFDM symbol interval $\lambda\in$[-0.5,0.5]. Its range (L, λ_d) is related to (τ,f_d) of $S_c(\tau,v)$ through $L = \lceil \tau_m B \rceil$ and $\lambda_d=f_dT_b$. This leads $G_{n,k}(d)$ to be a WSS but non-US fading channel [18].

$$
E\left\{G_{n',k'}(d)G_{n,k}^{*}(d)\right\} = Q(d,f_k)Q^{*}(d,f_{k'})R_H\left[n-n',k-k'\right] \tag{18}
$$

where $R_H\left[n-n',k-k'\right] = E\left[H_{n,k}H_{n,k}^{*}\right]$. Compared to the conventional WSSUS model (uncorrelated in both delay and Doppler domains), the proposed model is still uncorrelated in

Doppler but correlated in the delay domain because of attenuation. To be consistent, a vector form for $G_{n,k}(d)$ from (14) is

$$\mathbf{G}_n(d) = \mathbf{Q}(d)\mathbf{H}_n \tag{19}$$

where $\mathbf{Q}(d) = \mathrm{diag}\left(\left[Q(d, f_0)...Q(d, f_{K-1})\right]\right)$ and $\mathbf{H}_n = \left[H_{n,0}...H_{n,K-1}\right]^T$ from (15). Fig 2 shows a realization of $\left|G_{n,k}(d)\right|^2$ when d=5 and 20 km. $H_{n,k}$ is assumed zero-mean complex Gaussian random variable with exponentially decaying PDP with 20-dB power difference between the first and last paths. Transmit bandwidth is 51.2 kHz. Channel delay length is 5 ms which corresponds to L=256. The number of subcarriers K is 512. We can see that the propagation distance and signal frequency have a significant impact on the realization of $\left|G_{n,k}(d)\right|^2$.

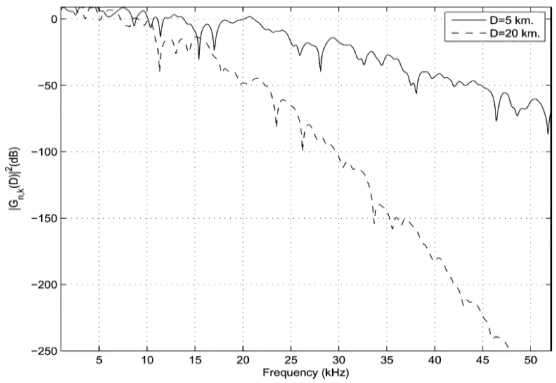

Fig. 2. Impact of attenuation on CIR

C. Ambient Noise

$N_{n,k}$ in (1) is assumed the ambient noise in the ocean which consists of four sources [6]: turbulence $A_t(f)$, shipping $A_s(f)$, waves $A_w(f)$, and thermal noise $A_{th}(f)$, described by Gaussian statistics with a continuous PSD in dBre/μPa per hertz,

$$\begin{aligned} A_t(f) &= 17 - 30\log f \\ A_s(f) &= 40 + 20(s - 0.5) + 26\log f - 60\log(f + 0.03) \\ A_w(f) &= 50 + 7.5\sqrt{w} + 20\log f - 40\log(f + 0.4) \\ A_{th}(f) &= -15 + 20\log f \end{aligned} \tag{20}$$

where f is the frequency in kilohertz, $s \in [0,1]$ is the shipping activity, w is the wind speed in meters per second, and overall noise PSD is

$$A(f) = 10\log\left(10^{A_t(f)/10} + 10^{A_s(f)/10} + 10^{A_w(f)/10} + 10^{A_{th}(f)/10}\right) \tag{21}$$

III. CAPACITY OF THE UW CHANNELS

The upper bound $U_c(d)$ and lower bound $L_c(d)$ are derived as a function of distance d between the transmitter and receiver. The capacity $C(d)$ is given in bits per second by

$$C(d) = \lim_{N\to\infty} \frac{1}{NT_b} \sup_{p(\mathbf{X})} I(\mathbf{Y};\mathbf{X}) \tag{22}$$

where the maximization is over the set $p(\mathbf{X})$ of all input distributions that satisfy a given average-power constraint. $U_c(d)$ is obtained when the input vector follows a join complex Gaussian distribution. $L_c(d)$ is obtained under imperfect CSI whose reduction from $U_c(d)$ comes from limited mutual information from PSK constellation and the MMSE prediction error related to channel uncertainty [12], [14]. This bounding technique is used in [12] for wireless fading channels while this paper uses it for UW channels. The bounds are derived under the following assumptions:

- Information of attenuation (7) and ambient noise PSD (21) of UW channels are available at both the transmitter and receiver.
- For statistical part [$H_{n,k}$ (15)] of UW channels, its approximate CIR $h_{n,l}[0]$ is assumed a WSSUS random process with variance σ_l^2 where $\sum_l \sigma_l^2 = E\left[\left|H_{n,k}\right|^2\right] = 1$. Rayleigh and Rician fading are also considered. A scattering function which characterizes $H_{n,k}$ is available at the receiver.
- The noise vector $\mathbf{N} \sim \mathcal{CN}\left(\mathbf{0}, diag(\mathbf{A})\right)$. Where $\mathbf{A} = \left[\mathbf{A}_0 ... \mathbf{A}_{N-1}\right]^T$ and $\mathbf{A}_n = \left[A(f_0), ..., A(f_{K-1})\right]^T$.
- The impact of ICI is negligible compared to $A(f_k)$.

Let F denote the subcarrier spacing and $B=KF$, the signal bandwidth. P is the signal transmit power in dBre/μPa.

A. Upper Bound $U_c(d)$

To bound $\sup_{p(\mathbf{X})} I(\mathbf{Y};\mathbf{X})$, we use the chain rule $I(\mathbf{Y};\mathbf{X}) = I(\mathbf{Y};\mathbf{X},\mathbf{G}(d)) - I(\mathbf{Y};\mathbf{G}(d)\,|\,\mathbf{X})$. The output vector $\mathbf{Y}$ depends on the input vector $\mathbf{X}$ through $\mathbf{b}$=daig($\mathbf{X}$)$\mathbf{G}(d)$, so $I(\mathbf{Y};\mathbf{X},\mathbf{G}(d))=I(\mathbf{Y};\mathbf{b})$. The upper bound of I(Y;b) is achieved when the input $\mathbf{b} \sim \mathcal{CN}(\mathbf{0}, \mathbf{I} + \mathbf{R}_\mathbf{X}(d) \odot \mathbf{R}_\mathbf{G}(d))$. Where

$\mathbf{R}_{\mathbf{G}}(d) = E[\mathbf{G}(d)\mathbf{G}^H(d)]$. $\mathbf{R}_{\mathbf{X}}(d) = \text{diag}\left(\left[\mathbf{R}_{\mathbf{X}_0}(d),...,\mathbf{R}_{\mathbf{X}_{N-1}}(d)\right]\right)$ where

$\mathbf{R}_{\mathbf{X}_n}(d) = \text{diag}\left(\left[\sigma_x^2(d, f_0)...\sigma_x^2(d, f_{K-1})\right]\right)$ and $\sigma_x^2(d, f_k) = E\left[\left|X_{n,k}\right|^2\right]$.

The upper bound $U_c(d)$ is [27],

$$\begin{aligned} C(d) &\le \lim_{N\to\infty} \frac{1}{NT_b} \sup_{\mathbf{R}_{\mathbf{X}}(d)} \log\det\left(\mathbf{I} + \left(\mathbf{R}_{\mathbf{X}}(d) \odot \mathbf{R}_{\mathbf{G}}(d)\right)\text{diag}(\mathbf{A})^{-1}\right) \\ &\le \lim_{N\to\infty} \frac{1}{NT_b} \sup_{\mathbf{R}_{\mathbf{X}}(d)} \sum_{n=0}^{N-1}\sum_{k=0}^{K-1} \log\left(1 + E\left[\left|X_{n,k}\right|^2\right]\frac{Q^2(d, f_k)}{A(f_k)}\right) \\ &= \frac{1}{T_b}\sum_{k=0}^{K-1} \sup_{\sigma_x^2(d,f_k)} \log\left(1 + \sigma_x^2(d, f_k)\frac{Q^2(d, f_k)}{A(f_k)}\right) \\ &= U_c(d) \end{aligned} \tag{23}$$

where the inequality follows from Hadamard's inequality [11]. This result is similar to [6] which is the capacity of time-invariant UW channels but is scaled by a factor of FT_b which is greater than 1 to avoid IBI. $\sigma_x^2(d, f_k)$ is subject to the source power constraint

$$F\sum_{k=0}^{K-1}\sigma_x^2(d, f_k) = P \tag{24}$$

U_c is obtained when energy allocation across all subcarriers satisfies

$$\sigma_x^2(d, f_k) = \begin{cases} \max\left(Th - \left(\frac{A(f_k)}{Q(d,f_k)^2}\right), 0\right) & f_k \in B \\ 0 & otherwise \end{cases} \tag{25}$$

where Th is chosen so that (24) is satisfied according to the water-filling algorithm [11].

B. Lower Bound $L_c(d)$ over Rayleigh Fading Channels

For lower bound, channel fading statistics are assumed available at the receiver, not the transmitter. Our results show, for the first time, that decrease in $L_c(d)$ depends not only on the channel variations but also on the propagation distance d between the transmitter and receiver.

Consider $I(\mathbf{Y};\mathbf{X})$ where each entry of $\mathbf{X}$, $X_{n,k}$ is an i.i.d r.v. drawn from PSK modulation whose amplitude $\left|X_{n,k}\right| = \sigma_x$ and phase $\angle X_{n,k}$ has a uniform discrete distribution across a circle. $I(\mathbf{Y};\mathbf{X})$ can be written as,

$$\begin{aligned} I(\mathbf{Y};\mathbf{X}) &= I\left(\mathbf{Y};\mathbf{X},\mathbf{G}(d)\right) - I\left(\mathbf{Y};\mathbf{G}(d)\,|\,\mathbf{X}\right) \\ &\ge I\left(\mathbf{Y};\mathbf{X}\,|\,\mathbf{G}(d)\right) - I\left(\mathbf{Y};\mathbf{G}(d)\,|\,\mathbf{X}\right) \end{aligned} \tag{26}$$

The inequality is due to the non-negativity property of mutual information. Exact calculation of the mutual information is infeasible due the non-Gaussian distribution of **Y** [28]. Note that [29]

$$I(\mathbf{Y};\mathbf{X}\,|\,\mathbf{G}(d)) = N\ I(\mathbf{Y}_N;\mathbf{X}_N\,|\,\mathbf{G}_N(d)) \tag{27}$$

where $\mathbf{G}_N(d)=\mathbf{G}_n(d)$, $\mathbf{X}_N=\mathbf{X}_n$, and $\mathbf{Y}_N=\mathbf{Y}_n$ since the input $X_{n,k}$ has an i.i.d. distribution and every block of the channel coefficients $\mathbf{G}_n(d)$ has the same distribution. $\sigma_x^2(d, f_k)$ is set according to (25) under constraint (24) and apply it to $I(\mathbf{Y}_N;\mathbf{X}_N\,|\,\mathbf{G}_N(d))$. This water-filling policy is suboptimal for PSK constellation [30]. $I(\mathbf{Y};\mathbf{G}(d)|\mathbf{X})$ is calculated in App. II which yields

$$I(\mathbf{Y};\mathbf{G}(d)\,|\,\mathbf{X}) = \sum_{n=0}^{N-1}\log\det\left(\mathbf{I}+\mathbf{B}_n(d)\,\mathrm{diag}\left(\mathbf{S}(d)\right)\right) \tag{28}$$

where $\mathbf{S}(d)$ is the $K\times 1$ vector whose kth entry is $\sigma_x^2(d, f_k)Q^2(d, f_k)/A(f_k)$. $\mathbf{B}_n(d)$ is the linear MMSE prediction error matrix which depends on both the transmission distance d and channel variation $R_H[m,k]$. Substituting (27) and (28) into (26), the mutual information is

$$I(\mathbf{X};\mathbf{Y}) \ge N\ I\left(\mathbf{Y}_N;\mathbf{X}_N\,|\,\mathbf{G}_N(d)\right) - \sum_{n=0}^{N-1}\log\det\left(\mathbf{I}+\mathbf{B}_n(d)\,\mathrm{diag}\left(\mathbf{S}(d)\right)\right) \tag{29}$$

Finally, the lower bound $L_c(d)$ of the capacity $C(d)$ can be written as,

$$\begin{aligned} C(d) &\ge \lim_{N\to\infty}\frac{1}{NT_b}I(\mathbf{Y};\mathbf{X}) \\ &\ge \frac{1}{T_b}I\left(\mathbf{Y}_\infty;\mathbf{X}_\infty\,|\,\mathbf{G}_\infty(d)\right) - \frac{1}{T_b}\log\det\left(\mathbf{I}+\mathbf{B}_\infty(d)\,\mathrm{diag}\left(\mathbf{S}(d)\right)\right) \\ &= L_c(d) \end{aligned} \tag{30}$$

where $\mathbf{B}_\infty(d)$ is calculated given infinite past channel symbols. From (30), unlike [12] and [19], channel scattering function is not explicit but lies within $\mathbf{B}_\infty(d)$.

C. Lower Bound $L_c(d)$ over Rician Fading Channels

Let ρ denote a Rician fading parameter which is the ratio of the fixed to a scatter part. ρ is assumed independent of the transmission distance d and identical for every delay path. The approximate CIR $h_{n,l}[0]$ of the lth path is modeled as

$$h_{n,l}[0] = \sigma_l\left(A_l e^{j\phi_l} + s_{n,l}\right) \tag{31}$$

$$\text{where } \rho = \frac{A_l^2}{E\left[\left|s_{n,l}\right|^2\right]} \qquad \text{and } A_l^2 = \frac{\rho}{\rho+1}, E\left[\left|s_{n,l}\right|^2\right] = \frac{1}{\rho+1} \tag{32}$$

$E\left[\left|h_{n,l}[0]\right|^2\right] = \sigma_l^2$. ϕ_l is assumed uniformly distributed from –π to π and uncorrelated across different delay paths. For $h(\mathbf{Y})$, using (31), $H_{n,k}$ is

$$H_{n,k} = \sum_{l=0}^{L-1} \sigma_l A_l e^{j\phi_l} e^{-j2\pi lk/K} + \sum_{l=0}^{L-1} \sigma_l s_{n,l} e^{-j2\pi lk/K} \tag{33}$$

From (33), sum of scatter part follows $\mathcal{CN}\left(0,1/(\rho+1)\right)$. This causes $H_{n,k} \sim \mathcal{CN}\left(D_k,1/(\rho+1)\right)$ where $Dk = \sum_{l=0}^{L-1} \sigma_l A_l e^{j\phi_l} e^{-j2\pi lk/K}$.

For $h(\mathbf{Y}|\mathbf{X})$, we assume that the receiver can successfully track the fixed part $A_l e^{j\phi_l}$ and the autocorrelation function of the approximate CIR is

$$E\left[h_{n,l}[0]h_{n',l'}^*[0]\right] = \left(A_l^2 + R_s\left[n-n',l\right]\right)\sigma_l^2\delta\left[l-l'\right] \tag{34}$$

Where $R_s\left[n-n',l\right] = E\left[s_{n,l}s_{n',l}^*\right]$. Apply (34) to calculate $\mathbf{B}_n(d)$ and obtain $h(\mathbf{Y}|\mathbf{X})$.

IV. Simulation results

The UW fading channel is modeled by two parts, attenuation and statistical as explained earlier. The delay profile is assumed exponentially decaying whose maximum delay spread τ_m is set where the first and last arrival paths have 10-dB power difference. The range of the Doppler profile scattering function is determined by f_d, the 3-dB bandwidth of the frequency response. For $A(f_k)$, the shipping activity s = 0.5 and wind speed w = 10 m/s. OFDM symbols are transmitter at frequency beyond 1 KHz. Energy allocation across transmit bandwidth $B_c(d)$ is implemented using (25) subject to power constraint (24). P=145 dBre/μPa and Rayleigh fading is assumed unless stated otherwise.

1) Limitations due to the ICI

Because of the attenuation, the variance of ICI is frequency dependent. This model assumes the ICI variance is negligible compared to that of the ambient noise. In simulation, the ICI variance is limited to at least 3 dB lower than ambient noise variance. The ICI variance depends

on attenuation, $\sigma_x^2(f_k)$, and shape of the scattering function. Two scattering functions, AR-1 and uniform scattering are considered whose 3 dB bandwidth is equal to λ_d. Let $S_1[l, \lambda]$ and $S_2[l, \lambda]$ denote these scattering functions of $h_{n,l}[0]$, respectively, given by

$$S_1[l,\lambda] = \frac{\sigma_l^2}{\left|1-\alpha_l e^{-j2\pi\lambda}\right|^2},\ \lambda \in [-0.5, 0.5]$$
$$S_2[l,\lambda] = \begin{cases} \frac{\sigma_l^2}{2\lambda_d}, & |\lambda| \le \lambda_d \\ 0, & \lambda_d < |\lambda| \le 0.5 \end{cases} \tag{35}$$

These scattering functions are assumed unchanged over the transmission ranges of interest. Fig. 3 displays variance of the ICI at their widest spread of both scattering functions when d=5 km such that its variance is at least 3 dB lower than that of the ambient noise for most of the transmission bandwidth. For the AR-1 model, τ_m =1 ms and f_d =1 Hz. For the uniform model, τ_m=5 ms and f_d =7 Hz. We notice that the 3-dB gap is violated when signal bandwidth is greater than 31 kHz. These account for only 0.39% of the total signal energy and have negligible impact on the capacity as justified in Appendix I.

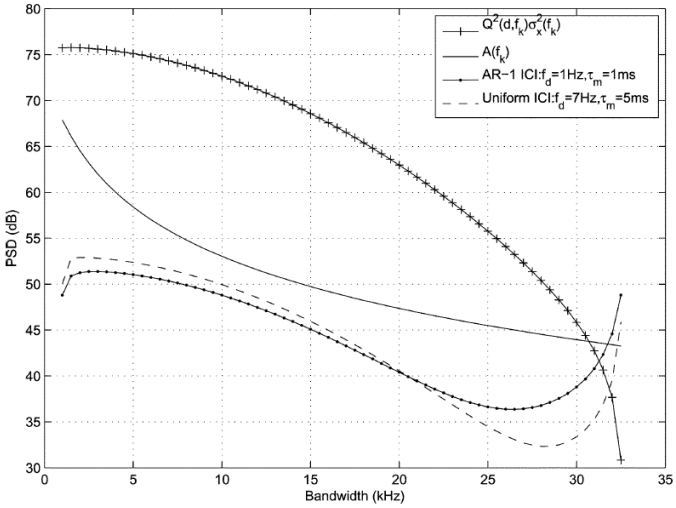

Fig. 3. PSD of the received signal, ambient noise, and the ICI variance at d=5 km

2) Impact of Signal Bandwidth

From Fig. 4, we can see that both $U_c(d)$ and $L_c(d)$ increase as a function of signal bandwidth B and remain fixed when B is greater than a certain value. We define this value as the capacity-maximizing bandwidth $B_c(d)$ which is a signal bandwidth that maximizes both $L_c(d)$ and $U_c(d)$. The gap beyond $B_c(d)$ is rather wide due to the limited mutual information that can be conveyed by the PSK constellation.

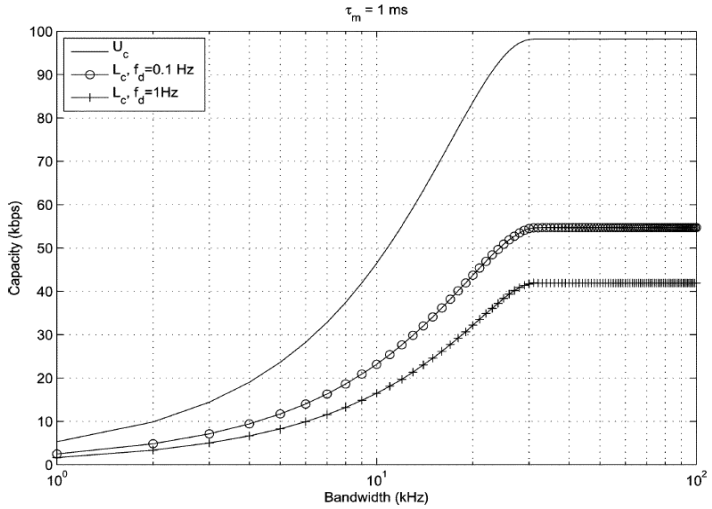

Fig. 4. $U_c(d)$ and $L_c(d)$ versus bandwidth for AR-1 model at d=5km

3) Impact of Ranges and Shape of the Scattering Function

Figs. 5 and 6 show the impact of the ranges of $(f_{d,}\tau_m)$ on $L_c(d)$ over the distance for $S_1[l, \lambda]$ and $S_2[l, \lambda]$, respectively.

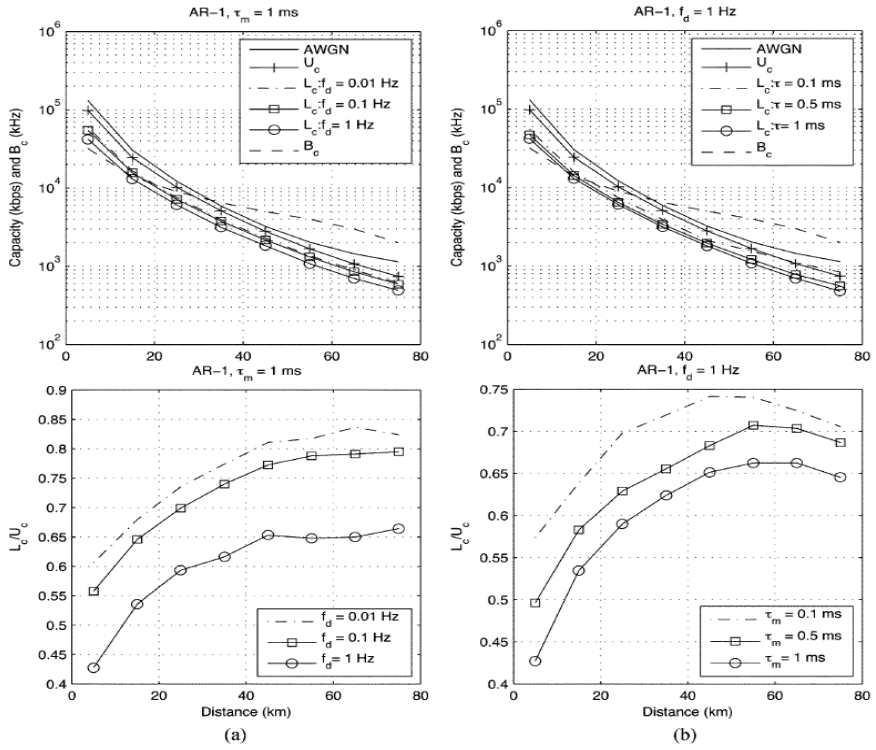

Fig. 5. Impact of (a) Doppler spread and (b) delay spread on $L_c(d)$ for AR-1 scattering function

As expected, the ratio between $L_c(d)$ and $U_c(d)$ increases as either f_d or τ_m increases. This is due to the higher prediction error influenced by stronger channel variations.

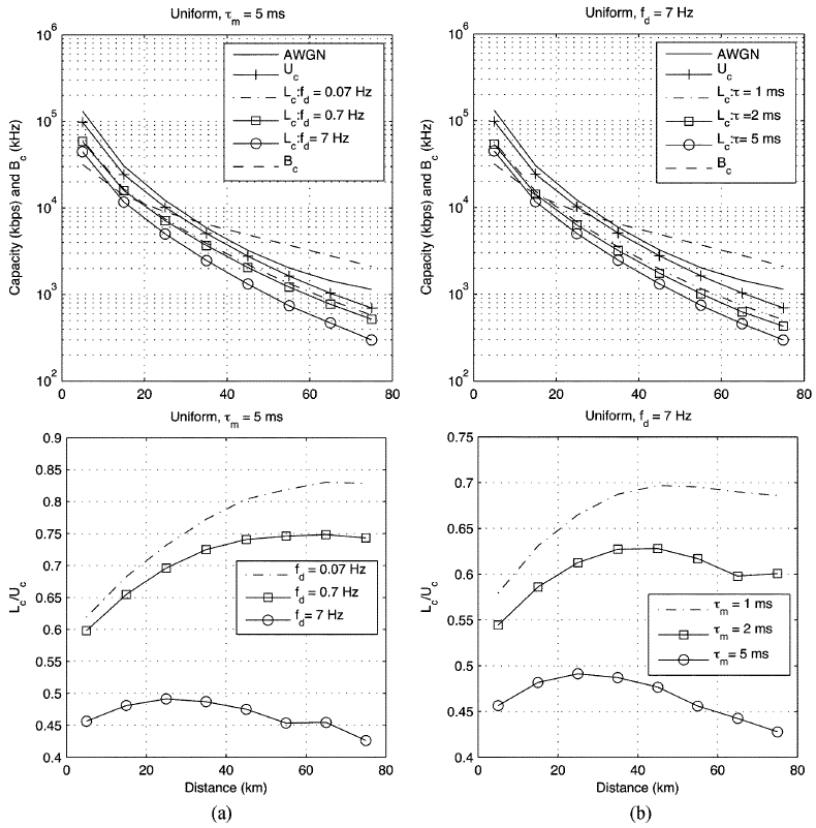

Fig. 6. Impact of (a) Doppler spread and (b) delay spread on $L_c(d)$ for uniform scattering

The impact of the shape of the scattering function is compared in Fig. 7 when f_d=1 Hz and τ_m=1 ms. We set F=500 kHz and T_b=15 ms. From the figure, $L_c(d)$ from $S_1[l, \lambda]$ is lower than that of $S_2[l, \lambda]$ as shown in Fig. 7(a). Fig. 7(b) shows the ratio of $L_c(d)$/ $U_c(d)$.

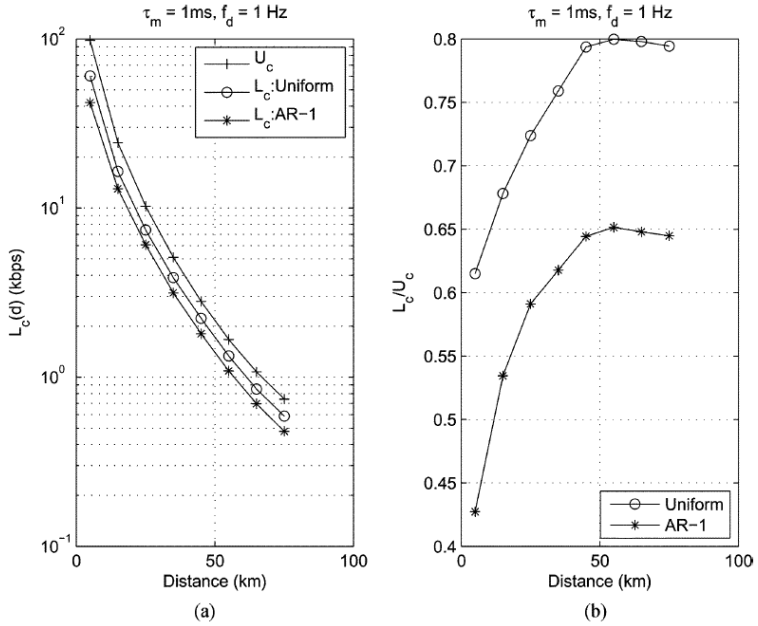

Fig. 7. Impact of the shape of scattering function on (a) $L_c(d)$ and (b) $L_c(d)$/ $U_c(d)$

4) Impact of Over Rician Fading Channels

The Ricean fading parameter ρ is set to -5, 0, 5, and 10 dB, identical for every path and independent of the distance. The Doppler spread profile of the scatter part (34) is assumed uniformly distributed. The fixed part is perfectly known at the receiver. From Fig. 8, the gap between the upper and lower bounds decreases as ρ increases which is due to the reduced power in the scatter part of the channel.

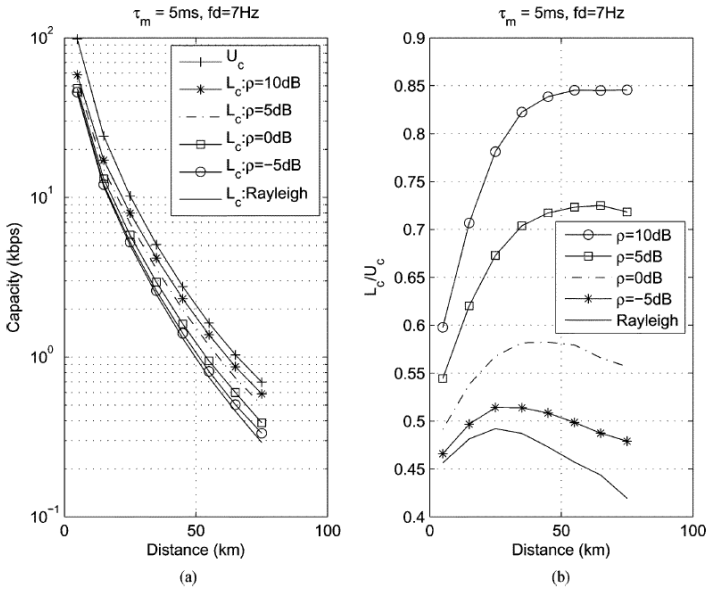

Fig. 8. $U_c(d)$ and $L_c(d)$ to the channel capacity over (a) Rician fading channel, (b) $L_c(d)/ U_c(d)$. Uniform Doppler spread profile

5) Impact of the Transmission Distance

From Figs. 5 and 6, both $L_c(d)$ and $U_c(d)$ decrease at longer distance owing to strong channel attenuation which determines $B_c(d)$. The gap at a short transmission distance is due to the energy wasted because of the PSK constellation while the gap at a very long distance is due to the higher prediction error because of the stronger attenuation.

6) Impact of Transmit Power

Fig. 9 shows the impact of transmit power on $L_c(d)$ and $B_c(d)$ for AR-1 scattering. A significant decrease in $L_c(d)$ and $B_c(d)$ occurs especially at long distance. This shows that for data transmission at low power, a short distance or multiple short hops across the transducers are preferred to one long transmission.

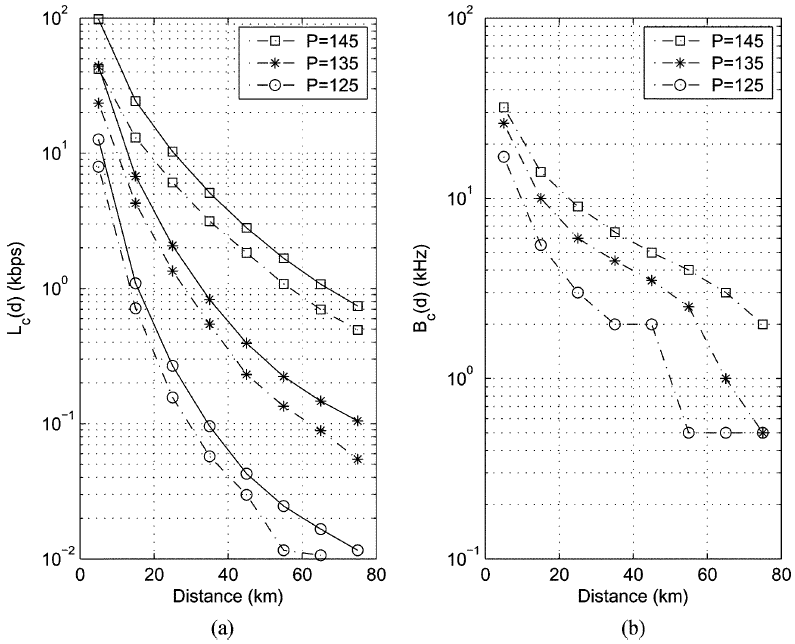

Fig. 9. Impact of transmit power on (a) $L_c(d)$ and (b) $B_c(d)$ for AR-1 scattering

V. EXPERIMENTAL DATA

The capacity of OFDM systems is investigated using the scattering function from real UW environments measured from the RACE08 experiment. Data is selected from the receiving arrays which are 1000 m from the transducer. The array is a 12-element vertical array with 12-cm spacing between elements. 8-PSK signals are upsampled by a factor of ten and filtered by a square root raised-cosine filter with a rolloff factor 0.25. A block of data which contain 64 data symbols are transmitted every 28.7 ms. A guard period is inserted between blocks to avoid the IBI. The bandwidth is 4.8 kHz at 12-kHz carrier frequency. Fig. 10(a) shows a contour plot of the estimates of the scattering function and Fig. 10(b) shows their corresponding PDP of process I–IV obtained from four different measurement periods.

Fig. 11(a) shows $L_c(d)$ and $U_c(d)$ from process I–IV over a range of the distance. Their corresponding $L_c(d)$ / $U_c(d)$ are displayed in Fig. 11(b). From the results, process II yields the best performance while process IV yields the worst. This is due to high Doppler spread at the dominant arrival paths in process IV while process II experiences smallest Doppler spread for almost every arrival path as shown in Fig. 10. Processes I and III exhibit similar results although process III is slightly worse since more dominant paths experience stronger Doppler spread compared to process I.

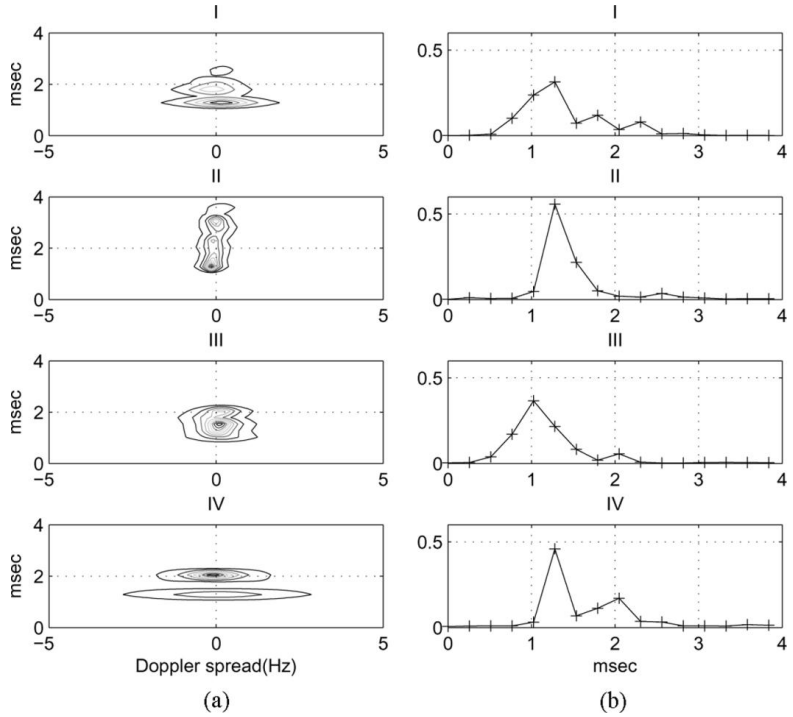

Fig. 10. (a) Scattering function estimates and (b) corresponding normalized PDP

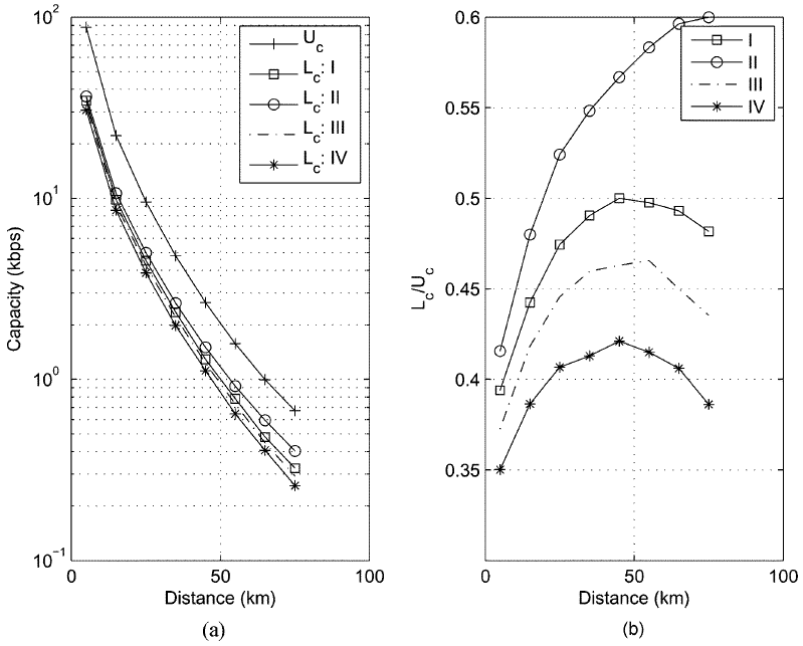

Fig. 11. (a) $L_c(d)$ $U_c(d)$ and (b) corresponding $L_c(d)/ U_c(d)$ over experimental UW fading channels

VI. DISCUSSION

After meeting, please write discussion in the meeting and update your presentation file.

Appendix

A. ICI Justification

To investigate the ICI impact, a simulation is run assuming that the ICI behaves as an independent complex Gaussian r.v. Therefore, the total noise accumulated in the simulation is the ICI plus the ambient noise. From (1), by including the ICI, the received signal can be written as

$$\begin{aligned} Y_{n,k} &= G_{n,k}(d)X_{n,k} + C_{n,k} + N_{n,k} \\ &= G_{n,k}(d)X_{n,k} + Z_{n,k} \end{aligned} \tag{36}$$

where $Z_{n,k}$ is the complex Gaussian noise consisting of the ambient and ICI noise whose variance is $E\left[\left|C_{n,k}\right|^2\right] + A(f_k)$. Using this assumption, Fig. 12 shows the $U_c(d)$ and $L_c(d)$ bounds at 5 km distance between transmitter and receiver. This distance gives highest ICI variance since longer distance means higher attenuation resulting in lower ICI.

In conclusion, it is shown that by taking into account the ICI as an additive complex Gaussian noise, $U_c(d)$ is reduced by at most 5.89% while $L_c(d)$ is reduced by at most 3.03%. This reduction is quite small and has little impact on the overall performance, and justifies our ICI setting.

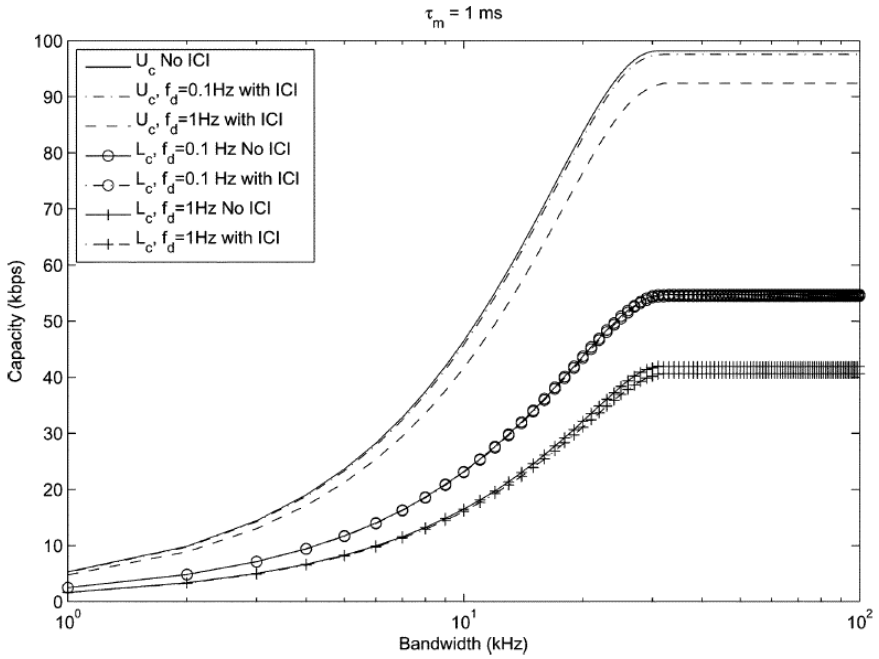

Fig. 12. Impact of ICI on $L_c(d)$ and $U_c(d)$ for AR-1 scattering function

B. I(Y;G(d)|X) Derivation

To calculate $I(\mathbf{Y};\mathbf{G}(d)|\mathbf{X})$, use the chain rule of differential entropy [11],

$$\begin{aligned} I\left(\mathbf{Y};\mathbf{G}(d)\,|\,\mathbf{X}\right) &= h\left(\mathbf{Y}\,|\,\mathbf{X}\right) - h\left(\mathbf{Y}\,|\,\mathbf{G}(d),\mathbf{X}\right) \\ &= h\left(\mathbf{Y}_0,\mathbf{Y}_1,...,\mathbf{Y}_{N-1}\,|\,\mathbf{X}\right) - N\sum_{k=0}^{K-1}\log\left(\pi eA(f_k)\right) \\ &= \sum_{n=0}^{N-1} h\left(\mathbf{Y}_n\,|\,\mathbf{Y}_0...\mathbf{Y}_{n-1},\mathbf{X}\right) - N\sum_{k=0}^{K-1}\log\left(\pi eA(f_k)\right) \end{aligned} \tag{37}$$

where

$$h\left(\mathbf{Y}_n\,|\,\mathbf{Y}_0...\mathbf{Y}_{n-1},\mathbf{X}\right) \triangleq \log\left(\left(\pi e\right)^K \det\left(\mathrm{Cov}\left[\mathbf{Y}_n\,|\,\mathbf{Y}_0...\mathbf{Y}_{n-1},\mathbf{X}\right]\right)\right) \tag{38}$$

To calculate $\mathrm{Cov}\left[\mathbf{Y}_n\,|\,\mathbf{Y}_0...\mathbf{Y}_{n-1},\mathbf{X}\right]$, we begin with mean

$$\begin{aligned} E\left[\mathbf{Y}_n\,|\,\mathbf{Y}_0...\mathbf{Y}_{n-1},\mathbf{X}\right] &= \mathrm{diag}(\mathbf{X}_n)E\left[\mathbf{G}_n(d)\,|\,\mathbf{Y}_n\,|\,\mathbf{Y}_0...\mathbf{Y}_{n-1},\mathbf{X}\right] \\ &= \left(\mathrm{diag}\left(\mathbf{X}_n\right)\mathbf{Q}(d)\right)\hat{\mathbf{H}}_n(d) \end{aligned} \tag{39}$$

Where (39) is obtained using (2) and (19). $\hat{\mathbf{H}}_n(d) = E\left[\mathbf{H}_n(d)\,|\,\mathbf{Y}_0,...,\mathbf{Y}_{n-1},\mathbf{X}\right]$ is the MMSE channel estimate given the current and past detected symbols and can be written as the 1-step output of the linear $K\times K$ MIMO predictor filter of length J

$$\hat{\mathbf{H}}_n(d) = \sum_{j=1}^{J} E_j(d)\tilde{\mathbf{H}}_{n-j}(d) \tag{40}$$

$\tilde{\mathbf{H}}_n(d) = \left[\tilde{H}_{n,0}(d)...\tilde{H}_{n,K-1}(d)\right]^T$ and $\mathbf{E}_j(d)$ is the predictor coefficient of size $K\times K$. With (1), the observation $\tilde{H}_{n,K-1}(d)$ is obtained by

$$\tilde{H}_{n,k}(d) = \frac{Y_{n,k}}{X_{n,k}Q(d,f_k)} = H_{n,k} + \frac{N_{n,k}}{X_{n,k}Q(d,f_k)} \tag{41}$$

Then from (39), $\mathrm{Cov}\left[\mathbf{Y}_n\,|\,\mathbf{Y}_0...\mathbf{Y}_{n-1},\mathbf{X}\right]$ is

$$\begin{aligned} &\mathrm{Cov}\left[\mathbf{Y}_n\,|\,\mathbf{Y}_0.s\mathbf{Y}_{n-1},\mathbf{X}\right] \\ &\triangleq E\left[\left(\mathbf{Y}_n - \left(\mathrm{daig}(\mathbf{X}_n)\mathbf{Q}(d)\right)\hat{\mathbf{H}}_n(d)\right)\times\left(\mathbf{Y}_n - \left(\mathrm{daig}(\mathbf{X}_n)\mathbf{Q}(d)\right)\hat{\mathbf{H}}_n(d)\right)^H\right] \\ &= \left(\mathrm{daig}(\mathbf{X}_n)\mathbf{Q}(d)\right)\mathbf{B}_n(d)\left(\mathrm{daig}(\mathbf{X}_n^*)\mathbf{Q}(d)\right) + \mathrm{diag}(\mathbf{A}_n) \end{aligned} \tag{42}$$

Where $\mathbf{B}_n(d)$ is the linear MMSE prediction error matrix obtained using the orthogonality principles.

Substituting (42) into (38) and into (37), $I(\mathbf{Y};\mathbf{G}(d)|\mathbf{X})$ is given as

$$\mathbf{I}(\mathbf{Y};\mathbf{G}(d)\,|\,\mathbf{X}) = \sum_{n=0}^{N-1} \log\det\left(\mathbf{I} + \mathrm{diag}\left(\mathbf{X}_n\right)\mathbf{B}_n(d)\,\mathrm{diag}\left(\mathbf{X}_n^*\right)\mathrm{diag}(\mathbf{A}_n)^{-1}\right)$$

$$= \sum_{n=0}^{N-1} \log\det\left(\mathbf{I} + \mathbf{B}_n(d)\,\mathrm{diag}\left(\mathbf{X}_n^*\right)\mathrm{diag}(\mathbf{A}_n)^{-1}\,\mathrm{diag}\left(\mathbf{X}_n\right)\right) \quad \because \det(\mathbf{I}+\mathbf{XY}) = \det(\mathbf{I}+\mathbf{YX}) \tag{43}$$

$$= \sum_{n=0}^{N-1} \log\det\left(\mathbf{I} + \mathbf{B}_n(d)\,\mathrm{diag}\left(\mathbf{S}(d)\right)\right)$$

The kth entry of the $K\times 1$ vector $\mathbf{S}(d)$ is $\sigma_x^2(d, f_k)Q^2(d, f_k) / A(f_k)$.

References

[1] Same as paper.

[2]